Article

Cell Reports

Structure of a Human 4E-T/DDX6/CNOT1 Complex Reveals the Different Interplay of DDX6-Binding Proteins with the CCR4-NOT Complex

Graphical Abstract

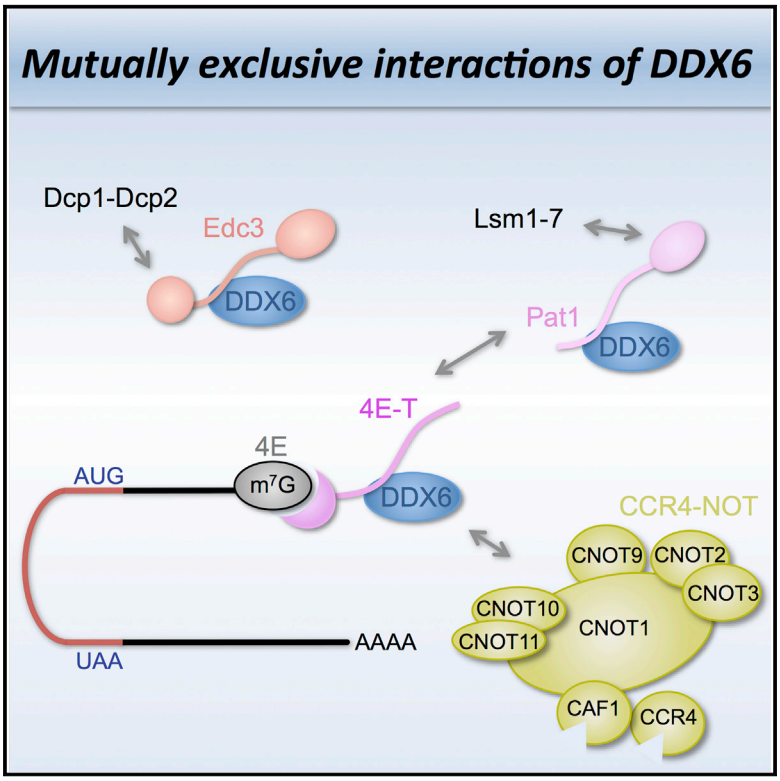

Authors

Sevim Ozgur, Jérôme Basquin, Anastasiia Kamenska, Witold Filipowicz, Nancy Standart, Elena Conti

Correspondence

conti@biochem.mpg.de

In Brief

Ozgur et al. show that 4E-T CHD binds DDX6 through the same surface as Edc3 and Pat1. However, only 4E-T can bind DDX6 together with the CNOT1 MIF4G domain. These findings provide insights into the complex network of interactions in DDX6-mediated translational repression.

Highlights

- DDX6 binds 4E-T, Pat1, and Edc3 using the same surfaces on the RecA2 domain
- DDX6 can bind 4E-T and the CNOT1 subunit of the CCR4-NOT complex simultaneously
- CNOT1 MIF4G binding impairs the interaction of DDX6 with Edc3 and Pat1 in vitro
- Localized electrostatic effects regulate the binding of related factors to CCR4-NOT

Accession Numbers

5ANR

Ozgur et al., 2015, Cell Reports *13*, 703–711
October 27, 2015 ©2015 The Authors
http://dx.doi.org/10.1016/j.celrep.2015.09.033

Cell Reports
Article

Structure of a Human 4E-T/DDX6/CNOT1 Complex Reveals the Different Interplay of DDX6-Binding Proteins with the CCR4-NOT Complex

Sevim Ozgur,[1] Jérôme Basquin,[1] Anastasiia Kamenska,[2] Witold Filipowicz,[3] Nancy Standart,[2] and Elena Conti[1,*]
[1]Department of Structural Cell Biology, Max-Planck-Institute of Biochemistry, Am Klopferspitz 18, 82152 Martinsried/Munich, Germany
[2]Department of Biochemistry, University of Cambridge, Tennis Court Road, Cambridge CB2 1QW, UK
[3]Friedrich Miescher Institute for Biomedical Research, Maulberstrasse 66, 4058 Basel, Switzerland
*Correspondence: conti@biochem.mpg.de
http://dx.doi.org/10.1016/j.celrep.2015.09.033

SUMMARY

The DEAD-box protein DDX6 is a central component of translational repression mechanisms in maternal mRNA storage in oocytes and microRNA-mediated silencing in somatic cells. DDX6 interacts with the CCR4-NOT complex and functions in concert with several post-transcriptional regulators, including Edc3, Pat1, and 4E-T. We show that the conserved CUP-homology domain (CHD) of human 4E-T interacts directly with DDX6 in both the presence and absence of the central MIF4G domain of CNOT1. The 2.1-Å resolution structure of the corresponding ternary complex reveals how 4E-T CHD wraps around the RecA2 domain of DDX6 and contacts CNOT1. Although 4E-T CHD lacks recognizable sequence similarity with Edc3 or Pat1, it shares the same DDX6-binding surface. In contrast to 4E-T, however, the Edc3 and Pat1 FDF motifs dissociate from DDX6 upon CNOT1 MIF4G binding in vitro. The results underscore the presence of a complex network of simultaneous and/or mutually exclusive interactions in DDX6-mediated repression.

INTRODUCTION

The CCR4-NOT complex is a conserved multi-protein assembly that impacts on eukaryotic gene expression at multiple levels and in organisms ranging from yeast to humans (Chapat and Corbo, 2014; Collart and Panasenko, 2012). In the cytoplasm, CCR4-NOT directly controls mRNA stability via the enzymatic activity of two of its core subunits, the CAF1 and CCR4 deadenylases (Tucker et al., 2001; Wahle and Winkler, 2013). Deadenylation is generally the first and rate-limiting step in mRNA turnover: once the 3′ poly(A) tail has been sufficiently shortened, the 5′ cap structure is removed, and the body of the transcript is swiftly degraded (Chen and Shyu, 2011; Garneau et al., 2007; Wahle and Winkler, 2013). Shortening of the poly(A) tail not only stimulates decay but also indirectly reduces translation by disrupting the association of the poly(A)-binding protein (PABP) and its interactions with the eukaryotic translation initiation factor 4F (eIF4F) (Kapp and Lorsch, 2004). However, CCR4-NOT also appears to control translational efficiency directly. Tethering assays have shown that the recruitment of CCR4-NOT to reporter mRNAs represses their translation in the absence of deadenylation, both in frog oocytes (Cooke et al., 2010) and upon miRNA-mediated gene silencing in human cells (Braun et al., 2011; Chekulaeva et al., 2011; Fabian et al., 2011). The first physical link between these different pathways centered at CCR4-NOT has been recently identified in the direct interaction between the scaffolding core subunit of the deadenylase complex, CNOT1, and a known translational repressor and decapping activator, DDX6 (Chen et al., 2014; Mathys et al., 2014; Rouya et al., 2014).

DDX6 proteins were originally characterized in *Drosophila melanogaster* with the discovery of Me31B, a factor involved in embryonic development. *Drosophila* Me31B represses the translation of maternal mRNAs during their transport to the oocyte (Nakamura et al., 2001) and is important for neuronal activity in adult flies, where it localizes in neuronal granules and controls translation at synapses (Barbee et al., 2006). Similarly, the *Caenorhabditis elegans* and *Xenopus laevis* orthologs (known as Chg-1 and Xp54) are found in germline granules and repress the translation of maternal mRNAs that are stored in these large ribonucleoprotein particles (RNPs) for subsequent activation (Boag et al., 2008; Ladomery et al., 1997). In humans, DDX6 (also known as RCK) is expressed in a variety of tissues (Lu and Yunis, 1992), is connected to chromosomal aberrations in several cancers (Robert and Pelletier, 2013), and participates as a translational repressor in different pathways, including mRNA storage in erythropoiesis (Ostareck-Lederer and Ostareck, 2012) and microRNA (miRNA)-mediated gene silencing (Chen et al., 2014; Chu and Rana, 2006; Mathys et al., 2014; Rouya et al., 2014). Finally, the *Saccharomyces cerevisiae* ortholog Dhh1 is able to repress translation (Carroll et al., 2011; Coller and Parker, 2005), but its best studied function is in the enhancement of mRNA decapping and decay (Coller et al., 2001; Fischer and Weis, 2002). In tissue culture cells, all DDX6 orthologs studied to date localize in RNP aggregates known as processing (P)-bodies, which also contain RNA decay factors (Anderson and Kedersha, 2006; Eulalio et al., 2007; Sheth and Parker, 2006).

DDX6 is a very abundant protein that belongs to the DEAD-box family of RNA-dependent ATPases (Ozgur et al., 2015; Presnyak

and Coller, 2013; Russell et al., 2013). It features the characteristic tandem of RecA-like domains (RecA1 and RecA2) but also has the unusual property of existing primarily in an autoinhibited conformation that can bind RNA in a non-productive, ATP-independent manner (Cheng et al., 2005; Dutta et al., 2011; Sharif et al., 2013). DDX6 coats repressed mRNA and has a potential to oligomerize (Ernoult-Lange et al., 2012). The ATPase activity of DDX6 is stimulated upon binding to the central MIF4G domain of CNOT1, which primes DDX6 toward its active conformation (Mathys et al., 2014). DDX6 activity is essential for miRNA silencing (Chen et al., 2014; Mathys et al., 2014; Rouya et al., 2014) and for P-body assembly (Minshall et al., 2009; Ozgur and Stoecklin, 2013). Paradoxically, the RecA2 domain alone is sufficient for translational repression in tethering assays (Minshall et al., 2009). This may be a consequence of the RecA2 domain of DDX6 having the ability to interact with other regulatory proteins. Edc3 and the Edc3-related protein Lsm14 (also known as Tral, Scd6, or RAP55) interact with DDX6 RecA2 through their Phe-Asp-Phe (FDF) motifs (Tritschler et al., 2008). In turn, Edc3 and Lsm14 directly bind and activate the decapping complex, DCP1-DCP2 (Fromm et al., 2012; Nissan et al., 2010; Tritschler et al., 2008). DDX6 also uses the same Edc3/Lsm14-binding surface to interact with Pat1 (Sharif et al., 2013), another modulator of mRNA stability and translation (Marnef and Standart, 2010).

Several lines of evidence point to 4E-T (eIF4E transporter) as a key translational repressor closely connected to DDX6. Biochemical studies in early *Xenopus* oocytes have shown that 4E-T co-purifies with Xp54/DDX6, Pat1, Lsm14, and the cap-binding protein eIF4E as part of a messenger RNP (mRNP) that stores silenced maternal mRNAs (Minshall et al., 2007). The *D. melanogaster* and *C. elegans* orthologs (CUP and IFET-1) also function as translational repressors acting in early development (Nakamura et al., 2004; Nelson et al., 2004; Sengupta et al., 2013). Similarly, 4E-T represents an essential component of the translation repressive complex in mouse neuronal progenitors (Yang et al., 2014). In tether-function studies, human 4E-T and *Drosophila* CUP inhibit the translation of reporter mRNAs to a level comparable to that of DDX6 (Ferraiuolo et al., 2005; Igreja and Izaurralde, 2011; Kamenska et al., 2014a). This protein family contains a canonical eIF4E-binding motif, analogous to that used by a diverse group of translational repressors for sequestering eIF4E, disrupting the eIF4F complex and impairing translation initiation (Kamenska et al., 2014b). Surprisingly, however, 4E-T and CUP can exert their repressive activity even independently from eIF4E (Igreja and Izaurralde, 2011; Kamenska et al., 2014a). The mechanism underlying 4E-independent translational repression is currently unclear. Here, we used biochemical and structural approaches to understand how DDX6 might function, together with 4E-T, in the context of the CCR4-NOT complex and of the DDX6-binding proteins Edc3 and Pat1.

RESULTS AND DISCUSSION

The Conserved CHD Region of 4E-T Interacts with the RecA2 Domain of DDX6

4E-T and DDX6 are found together spatially and temporally in different biological contexts (Kamenska et al., 2014b; Presnyak and Coller, 2013). We performed co-immunoprecipitation (co-IP) assays in human HEK293T cells. We transiently expressed yellow fluorescent protein (YFP)-tagged 4E-T and hemagglutinin (HA)-tagged DDX6, either wild-type or mutants (Figure 1B), and used GFP-binder beads for the precipitations. In these assays, DDX6 interacted with 4E-T (Figure 1B). The RecA2 domain of DDX6 is an interaction hotspot for different proteins. It contains an FDF-binding surface (the so-called patch 1 surface) that binds the FDF motifs of Edc3, Lsm14, and Pat1. Two other surfaces of DDX6 (known as patch 2 and patch 3) are also engaged in interactions with Edc3-related proteins and/or Pat1 (Sharif et al., 2013; Tritschler et al., 2009). We tested DDX6 mutants known to disrupt the interaction with both Edc3 and Pat1, namely, mutations in patch 1 (DDX6mut1) and patch 3 (DDX6mut3) (Sharif et al., 2013; Tritschler et al., 2009). We found that both abolished the interaction with 4E-T (Figure 1B). The RecA2 domain of DDX6 also interacts with CNOT1 (Chen et al., 2014; Mathys et al., 2014; Rouya et al., 2014). We tested a single amino acid substitution in DDX6 (DDX6mif3) that is known to abrogate binding to CNOT1 (Mathys et al., 2014). Importantly, DDX6mif3 did not affect the DDX6 interaction with 4E-T (Figure 1B). We concluded that the Edc3/Pat1-binding surfaces in the RecA2 domain of DDX6 are required for the interaction with 4E-T, while the CNOT1-binding surface of DDX6 is dispensable.

Human 4E-T is predicted to be largely unstructured. Besides the 4E-binding motif at the N terminus of the molecule (Dostie et al., 2000; Ferraiuolo et al., 2005) and a P-body localization region at the C terminus (Kamenska et al., 2014a), the most striking feature at the sequence level is a short segment that is highly conserved in the 4E-T family of proteins and has been termed the CUP-homology domain (CHD; residues 208–240) (Kamenska et al., 2014a) (Figure 1A). Another interesting region in the sequence of 4E-T is between residues 302 and 328, as it features an FDF-like motif (discussed later). Although the experiments in Figure 1B suggested that 4E-T is recognized at the FDF-binding site, a mutant of 4E-T whereby the FDF-containing motif had been removed still retained the ability to interact with DDX6 in co-IP assays (Figure 1C, 4E-T$_{\Delta FDF}$ mutant). Counterintuitively, removal of the CHD, which does not contain a recognizable FDF motif, decreased DDX6 binding to a larger extent (Figure 1C, 4E-T$_{\Delta CHD}$ mutant). Removal of both the CHD and FDF-like motifs of 4E-T had an additive effect in impairing the DDX6 interaction (Figure 1C). We concluded that the CHD is a major DDX6-binding segment of 4E-T. We note that the laboratory of Marc Fabian independently reached a similar conclusion in a recent paper (Nishimura et al., 2015) that was published while this manuscript was being reviewed.

Structure of the Ternary Complex of 4E-T CHD, DDX6, and CNOT1 MIF4G

We recapitulated the interactions observed in co-IP assays using in vitro reconstitutions with purified recombinant proteins. Human 4E-T CHD was co-expressed with the RecA2 domain of DDX6, and the two proteins were co-purified, forming a binary complex in size exclusion chromatography (Figure S1). Next, we tested the interaction with CNOT1. To this end, we co-expressed and co-purified a binary complex of 4E-T CHD and a DDX6 fragment containing both RecA domains (hereinafter referred to as

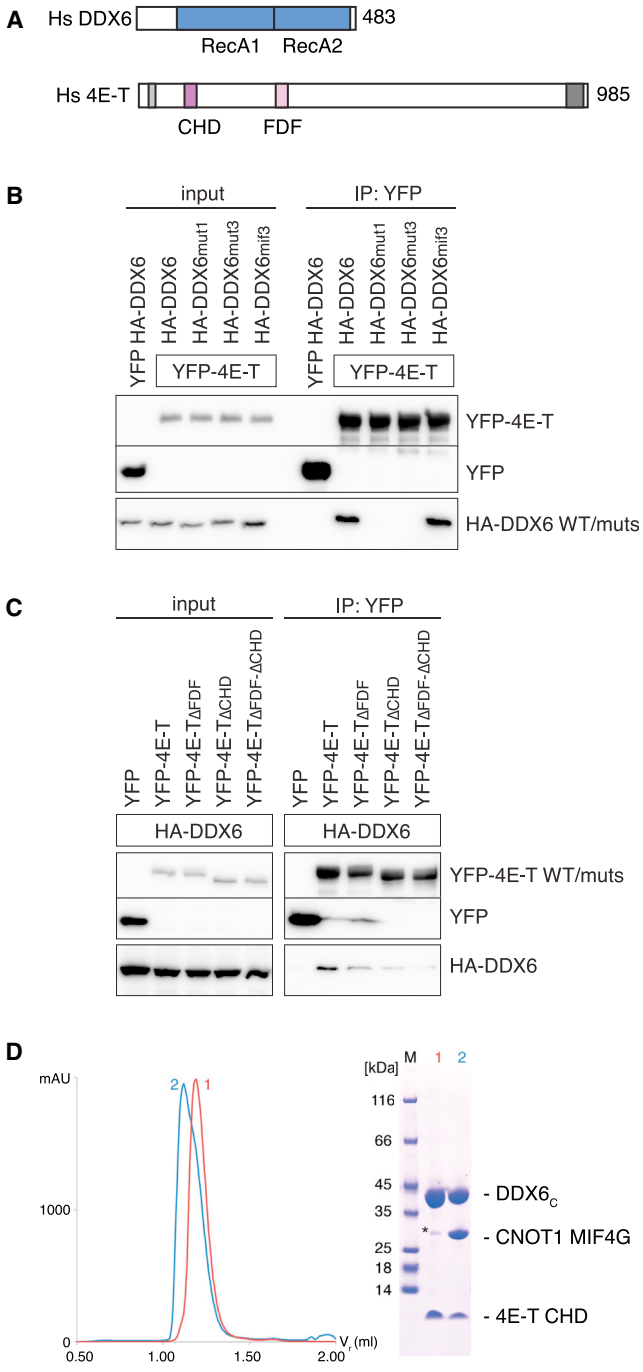

Figure 1. The 4E-T CHD Motif Interacts with the RecA2 Domain of DDX6

(A) Schematic representation of the domain arrangements of human DDX6 and 4E-T. In color are the portions of the molecules characterized in this study. The DEAD-box protein DDX6 has the two characteristic RecA domains (in blue). Within 4E-T, the CHD (residues 208–240, in magenta) and the FDF motif similar to that in Edc3 or Pat1 (FDF, residues 302–328, in pink) provide major and minor DDX6-binding sites, respectively. In light and dark gray are two other regions of 4E-T that have been previously characterized, namely, the N-terminal eIF4E-binding site and the C-terminal P-body localization site, respectively.

(B) Co-IP assays of *H. sapiens* HA-DDX6 with YFP-4E-T (in 150 mM NaCl). Wild-type and mutants were transiently transfected in HEK293T cells. Cell lysates (input) were immunoprecipitated with GFP binder, and eluted HA- and YFP-tagged proteins were detected by western blotting. DDX6mut1 (Q320A, H323A, T327A and R331A) impairs the FDF-binding site used for binding Pat1 and Edc3. DDX6mut3 (S343D, Q345D, and R346D) impairs a surface patch used for Pat1, but not Edc3, binding. DDX6mif3 (R386E) impairs CNOT1 binding. For the inability of these mutants to pull down Pat1, Edc3, or CNOT1, see Mathys et al. (2014), Sharif et al. (2013), and Tritschler et al. (2009).

(C) Co-IP of YFP-tagged 4E-T (either wild-type or mutants) with HA-tagged DDX6. The IP was done as described above, except that higher NaCl concentration (300 mM) was used in washes to better compare the relative contributions of the CHD and FDF motifs toward DDX6 binding. The deletion mutants 4E-T ΔCHD, ΔFDF, and ΔCHD-ΔFDF lack residues 208–240, 302–328, and 208–240 and 302–328, respectively.

(D) $DDX6_C$/4E-T interaction with recombinant proteins. $DDX6_C$ (residues 95–469) was co-expressed with the 4E-T CHD region (detailed in A), purified, and analyzed by size exclusion chromatography in the absence (peak 1) or presence (peak 2) of the CNOT1 MIF4G domain (Superdex 75_PC 3.2/300 column, GE Healthcare; exclusion volume, 0.8 ml). On the left are the overlays of the chromatograms (mAU and Vr denote relative absorbance and retention volume of the proteins, respectively). On the right is the Coomassie-stained SDS-PAGE gel with the samples from the corresponding peak fractions. Star indicates contamination.

See also Figure S1.

DDX6 core, or $DDX6_C$) and incubated it with a CNOT1 fragment encompassing the central MIF4G domain (hereinafter referred to as CNOT1 MIF4G). The three proteins co-eluted in size-exclusion chromatography, forming a 1:1:1 complex (Figure 1D). We determined the crystal structure of the 4E-T CHD/$DDX6_C$/CNOT1 MIF4G complex to a 2.1-Å resolution and refined it to an R_{free} of 23.2%, an R_{factor} of 19.3%, and good stereochemistry (Table 1). The final model includes residues 216–238 of 4E-T, residues 95–462 of DDX6, and residues 1065–1309 of CNOT1.

The structure of the $DDX6_C$/CNOT1 MIF4G portion of the ternary complex is similar to that of the binary complex previously described (Mathys et al., 2014). The MIF4G of CNOT1 has a crescent shape with a core that is formed by five tandem HEAT repeats. The convex surface of CNOT1 MIF4G that is used to interact with Caf1 (Basquin et al., 2012; Petit et al., 2012) is exposed to solvent (Figure 2, left panel). The concave surface of CNOT1 MIF4G faces $DDX6_C$ and uses the first and last HEAT repeats of the crescent to contact the RecA2 and RecA1 domains, respectively (Figure 2, left panel). Each RecA domain of $DDX6_C$ is formed of a flat, parallel β sheet sandwiched between two layers of α helices. The bottom of RecA2 (defined as the surface where the parallel β strands start) interacts with the B helix of MIF4G HEAT 1 using a pocket centered at DDX6 Arg386 (the residue substituted in the mif3 mutant discussed earlier). RecA1 contacts CNOT1 MIF4G at the B helix of HEAT 5 (Figure 2, left panel).

In the structure of the ternary 4E-T/$DDX6_C$/CNOT1 MIF4G complex, the two RecA domains of $DDX6_C$ face each other and are separated by ~10 Å. This conformation is essentially identical to that of the binary $DDX6_C$/CNOT1 MIF4G complex and is similar to the conformation adopted by the DEAD-box proteins eIF4A and Dbp5 when in complex with their MIF4G partners, eIF4G and Gle1 (Mathys et al., 2014; Montpetit et al., 2011; Schütz et al., 2008). As previously observed, this

Table 1. Data Collection and Refinement Statistics

Statistic	4E-T/CNOT1/DDX6
Wavelength (Å)	1
Resolution range (Å)[a]	47.32–2.102 (2.177–2.102)
Space group	P 32 2 1
Unit cell	93.129, 93.129, 175.329
α, β, γ (°)	90, 90, 120
Total reflections[a]	488,786 (34,933)
Unique reflections[a]	51,910 (5,023)
Multiplicity[a]	9.4 (7.0)
Completeness (%)[a]	99.74 (97.44)
Mean I/σ(I)[a]	17.61 (1.60)
CC1/2[a]	0.999 (0.806)
R_{merge}[a]	0.09499 (1.041)
R_{work}[a]	0.1931 (0.3400)
R_{free}[a]	0.2319 (0.3688)
Number of non-hydrogen atoms	
Total	5,205
Proteins	4,929
RMSD (bonds)	0.008
RMSD (angles)	1.09
Ramachandran favored (%)	97
Ramachandran outliers (%)	0.16
Average B factor	46.0

This table shows data collection and refinement statistics. Values for the highest resolution shell are given in parentheses. Structure validation was carried out with MolProbity (Chen et al., 2010). RMSD, root-mean-square deviation.

[a]Statistics for the highest resolution shell are shown in parentheses.

conformation approaches the structure that DEAD-box proteins adopt when in the active state (Mathys et al., 2014; Montpetit et al., 2011; Schütz et al., 2008) (Figure 2, right panel). In the active state, RNA is expected to bind in a shallow surface groove near the top surfaces of the two RecA domains, while ATP is expected to bind in a deep wedge on the opposite side of the molecule (Ozgur et al., 2015). 4E-T zig-zags around the N-terminal helical layer of RecA2 and contacts CNOT1 MIF4G.

4E-T CHD Interacts with DDX6 at the Same Hydrophobic Pockets Used by Edc3 and Pat1

4E-T CHD binds $DDX6_C$ in an extended conformation, burying more than 1,000 $Å^2$ of solvent-exposed area. The interaction is mediated by evolutionarily conserved amino acids (Figure 3A). Two hydrophobic residues of 4E-T (Ile233 and Leu235) bind the patch 1 surface of $DDX6_C$ via Van der Waals contacts with Cys324, Ile435, and Leu328 (Figure 3B, upper panel). 4E-T Ile233 and Leu235 are part of an IEL sequence motif and occupy the equivalent positions of the two phenylanine side chains in the FDF motifs of Edc3-related and Pat1 proteins (Figure 3B; Figure S2). In addition, the negatively charged residue in the IEL motif (Glu234) forms a salt bridge with $DDX6_C$ Arg331. Proceeding toward the C terminus of the CHD, 4E-T Phe238 binds part of the patch 2 surface of $DDX6_C$ via Van der Waals contacts with Tyr315. Edc3 orthologs from both human and yeast feature a phenylalanine residue at the equivalent position of 4E-T Phe238. However, the two proteins use different structural elements to cover the distance between patch 1 and patch 2 (an α-helix and a short glycine-containing segment, respectively) (Figure 3B; Figure S2).

Proceeding from the IEL motif toward the N terminus of the CHD, the 4E-T polypeptide chain makes a turn and wedges between two helices of RecA2, contacting CNOT1. Here, in addition to backbone-mediated interactions, the aliphatic portion of 4E-T Gln229 packs against the side chain of CNOT1 Phe1096. The 4E-T chain then folds into a short coil and inserts the side chains of Trp221 and Phe222 to interact with the patch 3 surface of $DDX6_C$ (formed by E318, H323, R346, L349, and K353) (Figure 3B). Both Edc3 and Pat1 orthologs feature a large aromatic residue at the equivalent position of 4E-T Trp221 (Figure 3B; Figure S2). Finally, at the N terminus of the CHD, a cluster of negatively charged amino acids binds near the top surface of the RecA2 domain (Figure 3B).

We concluded that 4E-T uses non-canonical sequence motifs to bind the same apolar pockets of $DDX6_C$ that are used for recognizing Edc3, Lsm14, and Pat1, rationalizing the effect of the DDX6 mutants shown in Figure 1B. Also, consistent with the structural analysis, 4E-T substitutions of Trp221Ala (4E-T_{Wmut}) or Trp221Ala, Phe222Ala (4E-T_{WFmut}) impaired DDX6 binding in co-IP assays (Figure 3C).

Flanking Residues in the FDF-like Motifs of DDX6-Binding Proteins Regulate the Interaction with CNOT1 MIF4G

The DDX6-binding domains of human Edc3 (residues 170–211) and Pat1 (residues 13–50) have been previously established (Sharif et al., 2013; Tritschler et al., 2009). We purified the corresponding Edc3/$DDX6_C$ and Pat1/$DDX6_C$ complexes and proceeded to add CNOT1 MIF4G. Unexpectedly, binding of CNOT1 MIF4G to $DDX6_C$ resulted in the dissociation of both Edc3 and Pat1 (Figures 4A and 4B). Careful comparison of the available structures of DDX6-bound complexes pointed to an interesting difference. In the case of 4E-T, the residue preceding the IEL motif is a conserved polar residue (Thr232), pointing toward a conserved negatively charged amino acid of CNOT1 (Glu1092) (Figure 4C). In the case of Edc3, Lsm14, and Pat1, the FDF motif is preceded by a conserved negatively charged residue (Asp203 for yeast Edc3, for example) (Figure 4C). Structural superpositions suggested that a negatively charged side chain at this position would result in electrostatic unfavorable interactions with CNOT1 Glu1092. To test this prediction, we engineered a Thr232Asp (T232D) substitution in 4E-T. In vitro, addition of CNOT1 MIF4G to the 4E-T T232D/$DDX6_C$ complex indeed displaced 4E-T (Figure 4D), suggesting that seemingly small differences in the sequence of different DDX6-binding proteins allow or disfavor binding when complexed with CNOT1 MIF4G. We note, however, that because of the multidomain organization of 4E-T and CNOT1 and their involvement in complex networks of protein-protein and protein-RNA interactions, there might be additional direct or indirect interaction sites outside the CNOT1 MIF4G. Indeed, the interaction of full-length 4E-T with

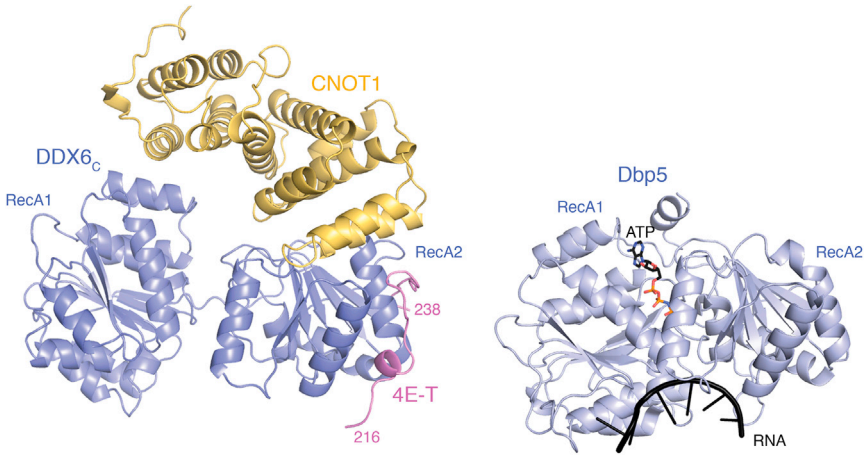

Figure 2. Structure of the Ternary Complex of DDX6$_C$, CNOT1 MIF4G, and 4E-T CHD

On the left, structure of the complex with the core of the DEAD-box protein DDX6, DDX6$_C$, in blue, 4E-T CHD in magenta, and the central MIF4G domain of CNOT1 in yellow. The N- and C-terminal residues of the 4E-T CHD region ordered in the structure are indicated. For comparison, on the right is the structure of a related DEAD-box protein, Dbp5, in the active conformation bound to and ATP analog and RNA (in black) (PDB: 3FHT) (von Moeller et al., 2009). The two structures are shown in the same orientation after optimal superposition of their RecA2 domains.

full-length CNOT1 was unaffected by the T232 substitution in 4E-T (Figure S3). This finding is consistent with recent observations of Nishimura et al. (2015) that the interaction of 4E-T with either DDX6 or CNOT1 can also be affected, either positively or negatively, by additional proteins such as Lsm14 and Pat1 (via their interaction with DDX6) or TTP (via its interaction with CNOT1). Furthermore, treatment of samples with RNase A during the co-IP assays resulted in stronger interaction with CNOT1 and reduced the DDX6 interaction (Figure S3). This observation suggests that, despite the direct interaction between 4E-T CHD and DDX6, mRNA has an important role in rearranging these interactions in vivo.

Conclusions

DDX6 functions in a wide range of translational repression pathways that ultimately lead to either mRNA degradation (e.g., in miRNA-mediated gene silencing) or mRNA storage (e.g., in germline and neuronal granules). It is currently thought that the different outcomes of translation repression might depend on the factors DDX6 binds to (Presnyak and Coller, 2013). Although DDX6 is similar to other DEAD-box proteins in terms of sequence and fold, it has distinctive surface features that underpin the direct interaction with specific regulatory proteins. One of the interacting proteins is the CNOT1 core subunit of the CCR4-NOT complex (Chen et al., 2014; Mathys et al., 2014; Rouya et al., 2014). The central MIF4G domain of CNOT1 regulates the catalytic activity of DDX6 by favoring the transition from the inactive to the active conformation of the ATPase (Mathys et al., 2014) and, at the same time, incorporates DDX6 to the CCR4-NOT complex. Another set of DDX6-interacting proteins includes Pat1 (Sharif et al., 2013), Edc3, Lsm14 (Tritschler et al., 2009), and—as shown here and also in other studies (Ayache et al., 2015; Nishimura et al., 2015)—4E-T. These proteins share several architectural features. First, they are mainly unstructured and presumably flexible. Second, they have a modular organization, with separate segments serving as platforms for protein-protein interactions, including association with DDX6. Importantly, our structural analysis has revealed that Pat1, Edc3, Lsm14, and 4E-T regulators are recognized by the same side surface of the DDX6 RecA2 domain.

The side surface of the DDX6 RecA2 domain is characterized by three hydrophobic hotspots. The most prominent hotspot (patch 1) was originally called the FDF-binding site because of the conserved short, interacting sequence motif found in Edc3 and Lsm14 (Tritschler et al., 2009). Although the CHD of 4E-T wraps around RecA2 with the same directionality observed in the case of Edc3 and Pat1 (threading from patch 3 to patch 1 and, finally, to patch 2), it lacks an FDF motif and, instead, uses different apolar sequence motifs connected by unrelated linker sequences to occupy the three hydrophobic hotspots. With hindsight, the interaction of 4E-T CHD could not be predicted by sequence analysis, and it is possible that, in the future, other proteins will be found to interact with DDX6 via "concealed" sequence motifs. The DDX6 CNOT1-binding region is adjacent to, but separate from, the side surface of RecA2. Our in vitro studies show that only 4E-T can interact with DDX6 concomitantly with the CNOT1 MIF4G domain. Surprisingly, Edc3 and Pat1 binding to DDX6 results in localized, unfavorable electrostatic effects, leading to their displacement upon binding of the CNOT1 MIF4G domain.

The implication of the mutually exclusive interactions identified from the structural analyses of DDX6 bound to Edc3 (Tritschler et al., 2009), Pat1 (Sharif et al., 2013), and 4E-T (the present article) is that a given DDX6 molecule can bind only one of the partners at a time. Different scenarios can be envisaged. In one model, the individual proteins could be recruited sequentially, with each binding event representing a progressive step in the pathway. For example, binding of 4E-T to DDX6 could occur first in the context of the CCR4-NOT complex. Following translational repression and deadenylation, Edc3 could displace 4E-T from DDX6 and tether DDX6 to the decapping complex (Fenger-Grøn et al., 2005; Tritschler et al., 2008). Pat1 binding to DDX6 would, instead, tether DDX6 to the Lsm1-7 complex (Ozgur et al., 2010; Sharif and Conti, 2013). In an alternative model, these interactions could reflect the existence of different complexes that perform related functions and that could exist either in isolation or in combination in large mRNP granules. This possibility is plausible because DDX6 is 10 to 20 times more abundant than other regulators (Beck et al., 2011; Nagaraj et al., 2011) and can thus participate in different complexes simultaneously. Importantly, our in vitro studies suggest that

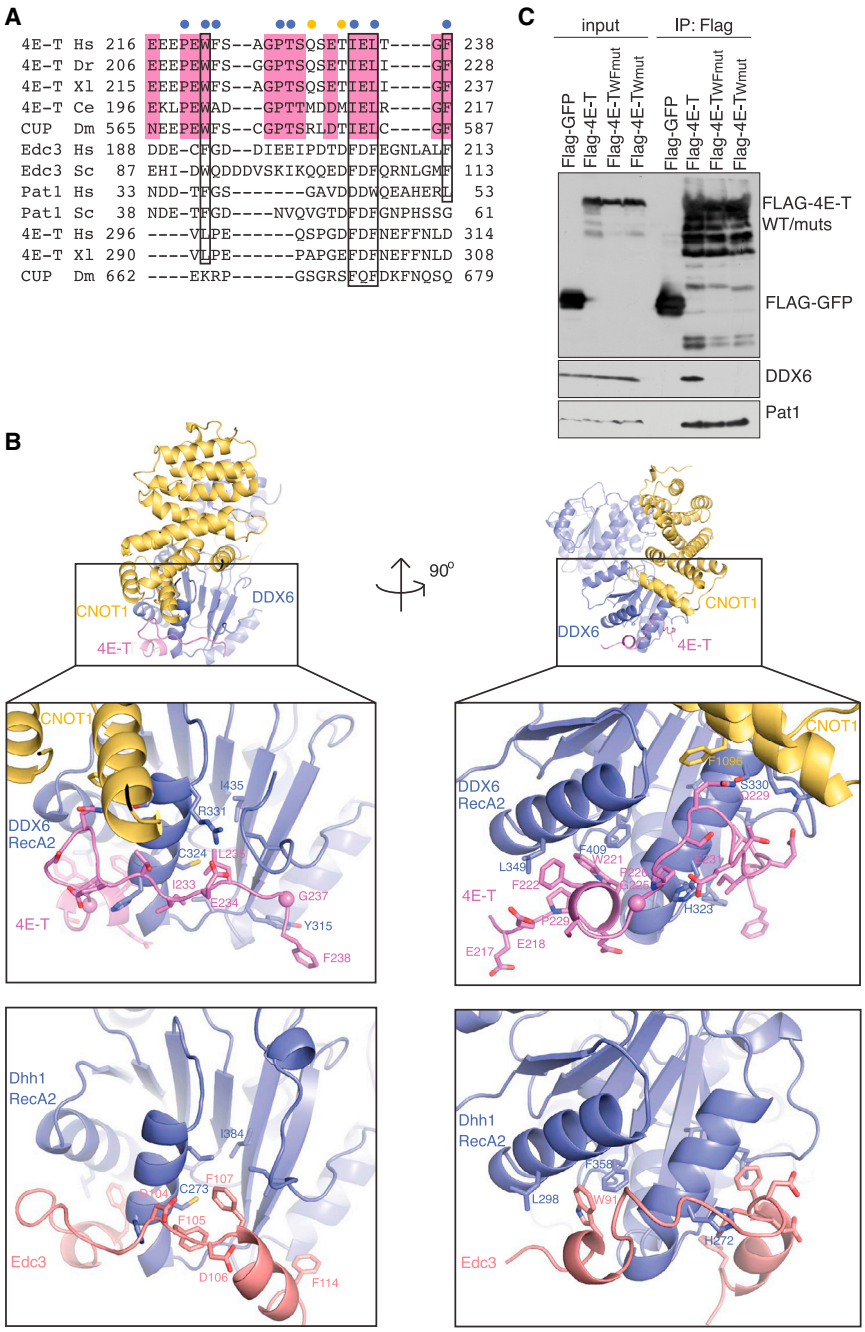

Figure 3. The 4E-T CHD Domain, Edc3, and Pat1 Bind at the Same Surfaces of DDX6

(A) Structure-based sequence alignment of the 4E-T CHD region from *H. sapiens* (Hs), *D. rerio* (Dr), *X. laevis* (Xl), *C. elegans* (Ce), and *D. melanogaster* (Dm) CUP. Conserved residues are highlighted in magenta boxes. Residues of 4E-T interacting with $DDX6_C$ and with CNOT1 MIF4G are indicated above the sequences with blue and yellow circles, respectively. The alignment also includes the DDX6-binding domains of Edc3 and Pat1 and of the 4E-T FDF region.

(B) Zoom-in of the interaction surfaces of 4E-T and $DDX6_C$/CNOT1 MIF4G in two orientations, with interacting residues in stick representation and labeled. The lower panels show the comparison with the interaction surfaces of yeast Edc3 and the yeast DDX6 ortholog Dhh1 (PDB: 4BRU), in the same orientations after optimal superposition.

(C) HEK293T cells were transiently transfected with FLAG-GFP, FLAG-4E-T, and FLAG-4E-T mutants WFmut (Trp221Ala, Phe222Ala) and Wmut (Trp221Ala). Lysates were immunoprecipitated using FLAG-M2 antibody beads, and eluted proteins were analyzed by SDS-PAGE followed by western blotting with indicated antibodies.

See also Figure S2.

only 4E-T (but neither Edc3 nor Pat1) would be able to bind DDX6 in the ATPase-competent conformation that is triggered by the interaction with the CNOT1 MIF4G domain. Finally, 4E-T is expected to interact not only with DDX6 and, indirectly, CNOT1 MIF4G via the CHD region but also with eIF4E cap-binding proteins via the N-terminal region and, as shown by Nishimura et al. (2015), with Pat1 and Lsm14 through other protein regions. The concomitant presence of multiple repressive complexes would provide redundancy and reinforce the robustness of translational repression.

Demonstration that 4E-T can associate with DDX6, even when the latter is in complex with the CNOT1 MIF4G, makes 4E-T a plausible candidate for the downstream effector in the GW182/CCR4-NOT/DDX6 axis, which functions in mediating translational repression by miRNAs. A role of DDX6 in repression of protein synthesis in the absence of mRNA deadenylation and/or decay, regardless of whether DDX6 is recruited to mRNA by the miRNA machinery or by direct tethering, is well documented (Carroll et al., 2011; Mathys et al., 2014; Minshall and Standart, 2004; Minshall et al., 2009; Presnyak and Coller, 2013). Likewise, 4E-T can inhibit protein synthesis in the absence of apparent mRNA degradation when tethered to mRNA, and, more importantly, its depletion was recently found to compromise repression of the miRNA reporter in human cells (Kamenska et al., 2014a). 4E-T was also identified as the translational repressor acting downstream of CNOT1 and DDX6 in *Xenopus* oocytes (Waghray et al., 2015).

In addition to its documented role in repression of translation, 4E-T has been shown to enhance decay of mRNAs bearing the 3′-UTR AU-rich elements (Ferraiuolo et al., 2005). The recent study of Nishimura et al. (2015) demonstrated that 4E-T, working together with DDX6 and CCR4-NOT, promotes mRNA decay by bridging the Lsm1-7/Pat1 complex associated with the mRNA 3′ terminus with the eIF4E bound to the 5′ cap. In the future, it will be

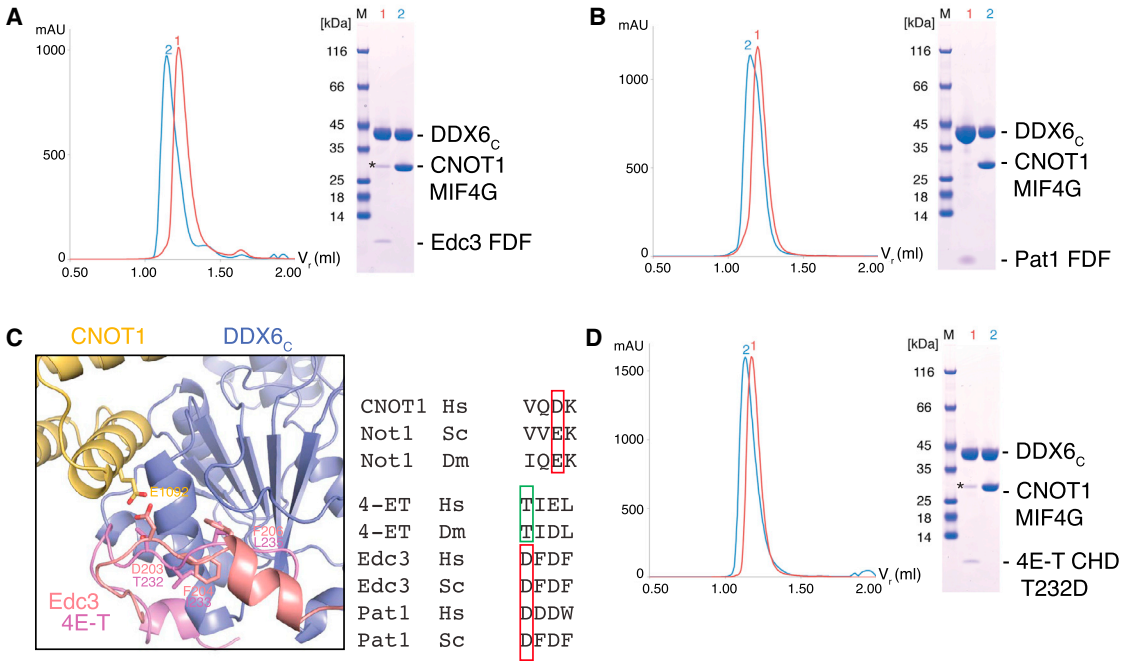

Figure 4. The 4E-T CHD Domain but Neither Edc3 Nor Pat1 Are Recruited to CNOT1 via DDX6

(A–D) In (A, B, and D), size exclusion chromatography assays assess formation of protein complexes. Purified samples of $DDX6_C$ and its interacting proteins (Edc3 FDF segment, Pat1 FDF-like segment, or 4E-T CHD T232D mutant) were incubated with CNOT1 MIF4G and co-injected on an analytical size exclusion chromatography column (Superdex 75_PC 3.2/300 column, GE Healthcare; exclusion volume 0.8 ml). On the left are the overlays of the chromatograms. On the right are the Coomassie-stained gels with samples from the corresponding peak fractions. Star indicates contamination. (C) Zoom-in at the FDF-binding site of $DDX6_C$. The structure of 4E-T/$DDX6_C$/CNOT1 MIF4G (with three proteins in magenta, blue, and yellow, respectively) is shown superposed on that of human Edc3 (in salmon) in complex with the RecA2 domain of DDX6 (PDB: 2WAX) (Tritschler et al., 2009). A conserved negatively charged residue of CNOT1 (E1092) is shown pointing toward Thr232 of 4E-T. At the corresponding position, Edc3 would feature a conserved negatively charged residue, Asp203. In the sequence alignment on the right, the corresponding residues are boxed in red or green, depending on whether they are negatively charged (red) or not (green).
See also Figure S3.

important to understand how the similar sets of factors, including proteins of the CCR4-NOT/DDX6/4E-T axis, are programmed to either inhibit translation or mediate mRNA decapping and decay. Likewise, it will be essential to establish the exact role of the CCR4-NOT/DDX6/4E-T pathway in translational silencing.

EXPERIMENTAL PROCEDURES

Protein Purification and Binding Assays

The expression vectors and purification protocols for human $DDX6_C$ (residues 95–469) and CNOT1 MIF4G domain (residues 1063–1314) were previously described (Mathys et al., 2014). Human 4E-T (residues 199–240) was cloned in a SUMO-tagged vector and co-expressed with DDX6 in BL21(DE3) pLyS in Terrific Broth (TB) medium. The 4E-T/$DDX6_C$ complex was co-purified using nickel-based affinity chromatography and ion-exchange chromatography at pH 7.5 (heparin, GE Healthcare), followed by tag cleavage by SENP2 and size exclusion chromatography (Superdex 75). $DDX6_C$/4E-T CHD was incubated with CNOT1 MIF4G in a 1.5:1 molar ratio and injected on a Superdex 75 in 20 mM Tris (pH 7.4), 250 mM NaCl, 1 mM DTT. Human Pat1 (residues 13–50), Edc3 (residues 170–211), and the 4E-T (residues 199–240) mutant T232D were co-expressed with $DDX6_C$ using analogous vectors and analogous protocols. The binding assays were performed by size exclusion chromatography as described for 4E-T.

Crystallization and Structure Determination

Crystallization was carried out at 4°C using the vapor diffusion method by mixing equal volumes of protein complex at 12 mg/ml and of crystallization buffer. The best diffracting crystals of 4E-T CHD/$DDX6_C$/CNOT1 MIF4G complex were obtained in 50 mM Tris (pH 8.0), 35% MPD (2-methyl-2,4-pentanediol), after 5 days. Crystals were flash frozen in liquid nitrogen directly from the crystallization drop and diffracted to a 2.1-Å resolution. Diffraction data were collected at 100 K at the beamline X06D (PXIII) of the Swiss Light Source (SLS) synchrotron and processed using XDS (McCoy et al., 2007). The structures were determined by molecular replacement with the program Phaser (Kabsch, 2010), using the structure of CNOT1 MIF4G/$DDX6_C$ complex (4CT4) (Mathys et al., 2014) as the search model. The atomic model was built with the program Coot (Emsley et al., 2010) and refined with PHENIX (Adams et al., 2010). The data collection and refinement statistics are summarized in Table 1.

Co-IP Assays

Co-IP assays on Figure 1 were essentially performed as described previously (Sharif et al., 2013). For co-IP on Figure 3C, HEK293T cell lysates were incubated with anti-FLAG-M2 beads (Sigma Aldrich); after washing, bound proteins were eluted with SDS loading buffer. Western blotting analysis was performed with 15% SDS-PAGE. The following antibodies were used in the ECL Western Blotting Detection System (GE Healthcare): rabbit anti-DDX6 (Bethyl Laboratories, A300-461A), Pat1b (Marnef and Standart, 2010), and mouse anti-FLAG (Sigma, F3165).

ACCESSION NUMBERS

The accession number for the coordinates and structure factors of the 4E-T CHD/$DDX6_C$/CNOT1 MIF4G complex is PDB: 5ANR.

SUPPLEMENTAL INFORMATION

Supplemental Information includes Supplemental Experimental Procedures and three figures and can be found with this article online at http://dx.doi.org/10.1016/j.celrep.2015.09.033.

AUTHOR CONTRIBUTIONS

S.O. and J.B. solved the structure and carried out the biochemical experiments in Figures 1, 2, and 4A–4D; A.K. carried out the experiment in Figure 3C; E.C., N.S., and W.F. initiated the project; E.C., S.O., and J.B. wrote the manuscript.

ACKNOWLEDGMENTS

We thank the MPI Crystallization Facility for screenings and optimization and the beamline scientists at the SLS for excellent assistance with data collection. We also thank Hansruedi Mathys and members of our laboratories for discussions and critical reading of the manuscript. This study was supported by the Max Planck Gesellschaft, the European Commission (ERC Advanced Investigator Grant 294371 and Marie Curie ITN RNPnet), and grants from the Deutsche Forschungsgemeinschaft (DFG SFB646, SFB1035, GRK1721, FOR1680, and CIPSM to E.C.) and the Biotechnology and Biological Sciences Research Council (BBSRC) to N.S.

Received: May 26, 2015
Revised: August 5, 2015
Accepted: September 10, 2015
Published: October 15, 2015

REFERENCES

Adams, P.D., Afonine, P.V., Bunkóczi, G., Chen, V.B., Davis, I.W., Echols, N., Headd, J.J., Hung, L.-W., Kapral, G.J., Grosse-Kunstleve, R.W., et al. (2010). PHENIX: a comprehensive Python-based system for macromolecular structure solution. Acta Crystallogr. D Biol. Crystallogr. *66*, 213–221.

Anderson, P., and Kedersha, N. (2006). RNA granules. J. Cell Biol. *172*, 803–808.

Ayache, J., Bénard, M., Ernoult-Lange, M., Minshall, N., Standart, N., Kress, M., and Weil, D. (2015). P-body assembly requires DDX6 repression complexes rather than decay or Ataxin2/2L complexes. Mol. Biol. Cell *26*, 2579–2595.

Barbee, S.A., Estes, P.S., Cziko, A.-M., Hillebrand, J., Luedeman, R.A., Coller, J.M., Johnson, N., Howlett, I.C., Geng, C., Ueda, R., et al. (2006). Staufen- and FMRP-containing neuronal RNPs are structurally and functionally related to somatic P bodies. Neuron *52*, 997–1009.

Basquin, J., Roudko, V.V., Rode, M., Basquin, C., Séraphin, B., and Conti, E. (2012). Architecture of the nuclease module of the yeast Ccr4-not complex: the Not1-Caf1-Ccr4 interaction. Mol. Cell *48*, 207–218.

Beck, M., Schmidt, A., Malmstroem, J., Claassen, M., Ori, A., Szymborska, A., Herzog, F., Rinner, O., Ellenberg, J., and Aebersold, R. (2011). The quantitative proteome of a human cell line. Mol. Syst. Biol. *7*, 549.

Boag, P.R., Atalay, A., Robida, S., Reinke, V., and Blackwell, T.K. (2008). Protection of specific maternal messenger RNAs by the P body protein CGH-1 (Dhh1/RCK) during Caenorhabditis elegans oogenesis. J. Cell Biol. *182*, 543–557.

Braun, J.E., Huntzinger, E., Fauser, M., and Izaurralde, E. (2011). GW182 proteins directly recruit cytoplasmic deadenylase complexes to miRNA targets. Mol. Cell *44*, 120–133.

Carroll, J.S., Munchel, S.E., and Weis, K. (2011). The DExD/H box ATPase Dhh1 functions in translational repression, mRNA decay, and processing body dynamics. J. Cell Biol. *194*, 527–537.

Chapat, C., and Corbo, L. (2014). Novel roles of the CCR4-NOT complex. Wiley Interdiscip. Rev. RNA *5*, 883–901.

Chekulaeva, M., Mathys, H., Zipprich, J.T., Attig, J., Colic, M., Parker, R., and Filipowicz, W. (2011). miRNA repression involves GW182-mediated recruitment of CCR4-NOT through conserved W-containing motifs. Nat. Struct. Mol. Biol. *18*, 1218–1226.

Chen, C.Y.A., and Shyu, A.B. (2011). Mechanisms of deadenylation-dependent decay. Wiley Interdiscip. Rev. RNA *2*, 167–183.

Chen, V.B., Arendall, W.B., 3rd, Headd, J.J., Keedy, D.A., Immormino, R.M., Kapral, G.J., Murray, L.W., Richardson, J.S., and Richardson, D.C. (2010). MolProbity: all-atom structure validation for macromolecular crystallography. Acta Crystallogr. D Biol. Crystallogr. *66*, 12–21.

Chen, Y., Boland, A., Kuzuoğlu-Öztürk, D., Bawankar, P., Loh, B., Chang, C.-T., Weichenrieder, O., and Izaurralde, E. (2014). A DDX6-CNOT1 complex and W-binding pockets in CNOT9 reveal direct links between miRNA target recognition and silencing. Mol. Cell *54*, 737–750.

Cheng, Z., Coller, J., Parker, R., and Song, H. (2005). Crystal structure and functional analysis of DEAD-box protein Dhh1p. RNA *11*, 1258–1270.

Chu, C.-Y., and Rana, T.M. (2006). Translation repression in human cells by microRNA-induced gene silencing requires RCK/p54. PLoS Biol. *4*, e210.

Collart, M.A., and Panasenko, O.O. (2012). The Ccr4–not complex. Gene *492*, 42–53.

Coller, J., and Parker, R. (2005). General translational repression by activators of mRNA decapping. Cell *122*, 875–886.

Coller, J.M., Tucker, M., Sheth, U., Valencia-Sanchez, M.A., and Parker, R. (2001). The DEAD box helicase, Dhh1p, functions in mRNA decapping and interacts with both the decapping and deadenylase complexes. RNA *7*, 1717–1727.

Cooke, A., Prigge, A., and Wickens, M. (2010). Translational repression by deadenylases. J. Biol. Chem. *285*, 28506–28513.

Dostie, J., Ferraiuolo, M., Pause, A., Adam, S.A., and Sonenberg, N. (2000). A novel shuttling protein, 4E-T, mediates the nuclear import of the mRNA 5′ cap-binding protein, eIF4E. EMBO J. *19*, 3142–3156.

Dutta, A., Zheng, S., Jain, D., Cameron, C.E., and Reese, J.C. (2011). Intermolecular interactions within the abundant DEAD-box protein Dhh1 regulate its activity in vivo. J. Biol. Chem. *286*, 27454–27470.

Emsley, P., Lohkamp, B., Scott, W.G., and Cowtan, K. (2010). Features and development of Coot. Acta Crystallogr. D Biol. Crystallogr. *66*, 486–501.

Ernoult-Lange, M., Baconnais, S., Harper, M., Minshall, N., Souquere, S., Boudier, T., Bénard, M., Andrey, P., Pierron, G., Kress, M., et al. (2012). Multiple binding of repressed mRNAs by the P-body protein Rck/p54. RNA *18*, 1702–1715.

Eulalio, A., Behm-Ansmant, I., and Izaurralde, E. (2007). P bodies: at the crossroads of post-transcriptional pathways. Nat. Rev. Mol. Cell Biol. *8*, 9–22.

Fabian, M.R., Cieplak, M.K., Frank, F., Morita, M., Green, J., Srikumar, T., Nagar, B., Yamamoto, T., Raught, B., Duchaine, T.F., and Sonenberg, N. (2011). miRNA-mediated deadenylation is orchestrated by GW182 through two conserved motifs that interact with CCR4-NOT. Nat. Struct. Mol. Biol. *18*, 1211–1217.

Fenger-Grøn, M., Fillman, C., Norrild, B., and Lykke-Andersen, J. (2005). Multiple processing body factors and the ARE binding protein TTP activate mRNA decapping. Mol. Cell *20*, 905–915.

Ferraiuolo, M.A., Basak, S., Dostie, J., Murray, E.L., Schoenberg, D.R., and Sonenberg, N. (2005). A role for the eIF4E-binding protein 4E-T in P-body formation and mRNA decay. J. Cell Biol. *170*, 913–924.

Fischer, N., and Weis, K. (2002). The DEAD box protein Dhh1 stimulates the decapping enzyme Dcp1. EMBO J. *21*, 2788–2797.

Fromm, S.A., Truffault, V., Kamenz, J., Braun, J.E., Hoffmann, N.A., Izaurralde, E., and Sprangers, R. (2012). The structural basis of Edc3- and Scd6-mediated activation of the Dcp1:Dcp2 mRNA decapping complex. EMBO J. *31*, 279–290.

Garneau, N.L., Wilusz, J., and Wilusz, C.J. (2007). The highways and byways of mRNA decay. Nat. Rev. Mol. Cell Biol. *8*, 113–126.

Igreja, C., and Izaurralde, E. (2011). CUP promotes deadenylation and inhibits decapping of mRNA targets. Genes Dev. *25*, 1955–1967.

Kabsch, W. (2010). XDS. Acta Crystallogr. D Biol. Crystallogr. *66*, 125–132.

Kamenska, A., Lu, W.-T., Kubacka, D., Broomhead, H., Minshall, N., Bushell, M., and Standart, N. (2014a). Human 4E-T represses translation of bound mRNAs and enhances microRNA-mediated silencing. Nucleic Acids Res. *42*, 3298–3313.

Kamenska, A., Simpson, C., and Standart, N. (2014b). eIF4E-binding proteins: new factors, new locations, new roles. Biochem. Soc. Trans. *42*, 1238–1245.

Kapp, L.D., and Lorsch, J.R. (2004). The molecular mechanics of eukaryotic translation. Annu. Rev. Biochem. *73*, 657–704.

Ladomery, M., Wade, E., and Sommerville, J. (1997). Xp54, the Xenopus homologue of human RNA helicase p54, is an integral component of stored mRNP particles in oocytes. Nucleic Acids Res. *25*, 965–973.

Lu, D., and Yunis, J.J. (1992). Cloning, expression and localization of an RNA helicase gene from a human lymphoid cell line with chromosomal breakpoint 11q23.3. Nucleic Acids Res. *20*, 1967–1972.

Marnef, A., and Standart, N. (2010). Pat1 proteins: a life in translation, translation repression and mRNA decay. Biochem. Soc. Trans. *38*, 1602–1607.

Mathys, H., Basquin, J., Ozgur, S., Czarnocki-Cieciura, M., Bonneau, F., Aartse, A., Dziembowski, A., Nowotny, M., Conti, E., and Filipowicz, W. (2014). Structural and biochemical insights to the role of the CCR4-NOT complex and DDX6 ATPase in microRNA repression. Mol. Cell *54*, 751–765.

McCoy, A.J., Grosse-Kunstleve, R.W., Adams, P.D., Winn, M.D., Storoni, L.C., and Read, R.J. (2007). Phaser crystallographic software. J Appl Crystallogr *40*, 658–674.

Minshall, N., and Standart, N. (2004). The active form of Xp54 RNA helicase in translational repression is an RNA-mediated oligomer. Nucleic Acids Res. *32*, 1325–1334.

Minshall, N., Reiter, M.H., Weil, D., and Standart, N. (2007). CPEB interacts with an ovary-specific eIF4E and 4E-T in early Xenopus oocytes. J. Biol. Chem. *282*, 37389–37401.

Minshall, N., Kress, M., Weil, D., and Standart, N. (2009). Role of p54 RNA helicase activity and its C-terminal domain in translational repression, P-body localization and assembly. Mol. Biol. Cell *20*, 2464–2472.

Montpetit, B., Thomsen, N.D., Helmke, K.J., Seeliger, M.A., Berger, J.M., and Weis, K. (2011). A conserved mechanism of DEAD-box ATPase activation by nucleoporins and InsP6 in mRNA export. Nature *472*, 238–242.

Nagaraj, N., Wisniewski, J.R., Geiger, T., Cox, J., Kircher, M., Kelso, J., Pääbo, S., and Mann, M. (2011). Deep proteome and transcriptome mapping of a human cancer cell line. Mol. Syst. Biol. *7*, 548.

Nakamura, A., Amikura, R., Hanyu, K., and Kobayashi, S. (2001). Me31B silences translation of oocyte-localizing RNAs through the formation of cytoplasmic RNP complex during Drosophila oogenesis. Development *128*, 3233–3242.

Nakamura, A., Sato, K., and Hanyu-Nakamura, K. (2004). Drosophila cup is an eIF4E binding protein that associates with Bruno and regulates oskar mRNA translation in oogenesis. Dev. Cell *6*, 69–78.

Nelson, M.R., Leidal, A.M., and Smibert, C.A. (2004). Drosophila Cup is an eIF4E-binding protein that functions in Smaug-mediated translational repression. EMBO J. *23*, 150–159.

Nishimura, T., Padamsi, Z., Fakim, H., Milette, S., Dunham, W.H., Gingras, A.-C., and Fabian, M.R. (2015). The eIF4E-binding protein 4E-T is a component of the mRNA decay machinery that bridges the 5′ and 3′ termini of target mRNAs. Cell Rep. *11*, 1425–1436.

Nissan, T., Rajyaguru, P., She, M., Song, H., and Parker, R. (2010). Decapping activators in Saccharomyces cerevisiae act by multiple mechanisms. Mol. Cell *39*, 773–783.

Ostareck-Lederer, A., and Ostareck, D.H. (2012). Precision mechanics with multifunctional tools: how hnRNP K and hnRNPs E1/E2 contribute to post-transcriptional control of gene expression in hematopoiesis. Curr. Protein Pept. Sci. *13*, 391–400.

Ozgur, S., and Stoecklin, G. (2013). Role of Rck-Pat1b binding in assembly of processing-bodies. RNA Biol. *10*, 528–539.

Ozgur, S., Chekulaeva, M., and Stoecklin, G. (2010). Human Pat1b connects deadenylation with mRNA decapping and controls the assembly of processing bodies. Mol. Cell. Biol. *30*, 4308–4323.

Ozgur, S., Buchwald, G., Falk, S., Chakrabarti, S., Prabu, J.R., and Conti, E. (2015). The conformational plasticity of eukaryotic RNA-dependent ATPases. FEBS J. *282*, 850–863.

Petit, A.-P., Wohlbold, L., Bawankar, P., Huntzinger, E., Schmidt, S., Izaurralde, E., and Weichenrieder, O. (2012). The structural basis for the interaction between the CAF1 nuclease and the NOT1 scaffold of the human CCR4-NOT deadenylase complex. Nucleic Acids Res. *40*, 11058–11072.

Presnyak, V., and Coller, J. (2013). The DHH1/RCKp54 family of helicases: an ancient family of proteins that promote translational silencing. Biochim. Biophys. Acta *1829*, 817–823.

Robert, F., and Pelletier, J. (2013). Perturbations of RNA helicases in cancer. Wiley Interdiscip. Rev. RNA *4*, 333–349.

Rouya, C., Siddiqui, N., Morita, M., Duchaine, T.F., Fabian, M.R., and Sonenberg, N. (2014). Human DDX6 effects miRNA-mediated gene silencing via direct binding to CNOT1. RNA *20*, 1398–1409.

Russell, R., Jarmoskaite, I., and Lambowitz, A.M. (2013). Toward a molecular understanding of RNA remodeling by DEAD-box proteins. RNA Biol. *10*, 44–55.

Schütz, P., Bumann, M., Oberholzer, A.E., Bieniossek, C., Trachsel, H., Altmann, M., and Baumann, U. (2008). Crystal structure of the yeast eIF4A-eIF4G complex: an RNA-helicase controlled by protein-protein interactions. Proc. Natl. Acad. Sci. USA *105*, 9564–9569.

Sengupta, M.S., Low, W.Y., Patterson, J.R., Kim, H.-M., Traven, A., Beilharz, T.H., Colaiácovo, M.P., Schisa, J.A., and Boag, P.R. (2013). ifet-1 is a broad-scale translational repressor required for normal P granule formation in C. elegans. J. Cell Sci. *126*, 850–859.

Sharif, H., and Conti, E. (2013). Architecture of the Lsm1-7-Pat1 complex: a conserved assembly in eukaryotic mRNA turnover. Cell Rep. *5*, 283–291.

Sharif, H., Ozgur, S., Sharma, K., Basquin, C., Urlaub, H., and Conti, E. (2013). Structural analysis of the yeast Dhh1-Pat1 complex reveals how Dhh1 engages Pat1, Edc3 and RNA in mutually exclusive interactions. Nucleic Acids Res. *41*, 8377–8390.

Sheth, U., and Parker, R. (2006). Targeting of aberrant mRNAs to cytoplasmic processing bodies. Cell *125*, 1095–1109.

Tritschler, F., Eulalio, A., Helms, S., Schmidt, S., Coles, M., Weichenrieder, O., Izaurralde, E., and Truffault, V. (2008). Similar modes of interaction enable Trailer Hitch and EDC3 to associate with DCP1 and Me31B in distinct protein complexes. Mol. Cell. Biol. *28*, 6695–6708.

Tritschler, F., Braun, J.E., Eulalio, A., Truffault, V., Izaurralde, E., and Weichenrieder, O. (2009). Structural basis for the mutually exclusive anchoring of P body components EDC3 and Tral to the DEAD box protein DDX6/Me31B. Mol. Cell *33*, 661–668.

Tucker, M., Valencia-Sanchez, M.A., Staples, R.R., Chen, J., Denis, C.L., and Parker, R. (2001). The transcription factor associated Ccr4 and Caf1 proteins are components of the major cytoplasmic mRNA deadenylase in Saccharomyces cerevisiae. Cell *104*, 377–386.

von Moeller, H., Basquin, C., and Conti, E. (2009). The mRNA export protein DBP5 binds RNA and the cytoplasmic nucleoporin NUP214 in a mutually exclusive manner. Nat. Struct. Mol. Biol. *16*, 247–254.

Waghray, S., Williams, C., Coon, J.J., and Wickens, M. (2015). Xenopus CAF1 requires NOT1-mediated interaction with 4E-T to repress translation in vivo. RNA *21*, 1335–1345.

Wahle, E., and Winkler, G.S. (2013). RNA decay machines: deadenylation by the Ccr4–Not and Pan2–Pan3 complexes. Biochim. Biophys. Acta *1829*, 561–570.

Yang, G., Smibert, C.A., Kaplan, D.R., and Miller, F.D. (2014). An eIF4E1/4E-T complex determines the genesis of neurons from precursors by translationally repressing a proneurogenic transcription program. Neuron *84*, 723–739.